Geometry Optimization of Porous Electrode for Lithium-Ion Batteries

ECS Transactions, 97 (7) 249-254 (2020)
10.1149/09707.0249ecst ©The Electrochemical Society

Geometry Optimization of Porous Electrode for Lithium-ion Batteries

Changyu Deng[a], and Wei Lu[a,b]

[a] Department of Mechanical Engineering, University of Michigan, Ann Arbor, Michigan 48109, USA
[b] Department of Materials Science & Engineering, University of Michigan, Ann Arbor, Michigan 48109, USA

We report a method to optimize the topology of porous electrodes without a prior assumption of the pattern. We take a two-dimensional NMC-Li cell as an example. The domain of NMC is discretized by a 5×5 mesh and the solid volume fraction is represented by 25 nodal variables. We use a deep-learning-boosted optimization algorithm to find the optimal material distribution that gives the maximum specific energy. The method produces an electrode pattern with 18% higher energy than that of a uniform electrode. This generic geometry optimization approach provides a powerful tool for the design and optimization of porous electrodes.

Introduction

Since the invention of lithium-ion batteries about 40 years ago, the electrodes have been manufactured in essentially the same way: granulating active materials into powder, mixing them with additives such as carbon black and binder, and pasting them on a conductive substrate. Many researches on battery design optimization focus on tuning parameters such as particle size, porosity and electrode thickness for a flat, uniform electrode. Recent studies highlight that patterned electrodes, such as those with cylindrical nanowires[1], tunnels[2], and fractal electrodes[3], can offer better performance. However, it remains unknown what an optimized pattern should look like. An approach that enables optimizing the material distribution of a porous electrode without any prior assumption on its pattern is highly needed.

Here we report a method to optimize the topology of a porous electrode. A 2-dimensional NMC 333 electrode with lithium metal as the counter electrode is considered as an example. The material distribution of the porous electrode is no longer uniform, but can take any form. To find the optimal solid material distribution for maximum specific energy, we represent the NMC material distribution by 5×5 nodal design variables. This optimization problem with 25 parameters is solved by self-directed online machine learning, which couples deep neural network (DNN) and Generalized Simulated Annealing (GSA).[4]

Method

Let us consider a two-dimensional electrode as shown in Figure 1. The cell is composed of a Cu foil as the current collector, an NMC 333 porous electrode, a separator,

and a lithium metal electrode. The average solid volume fraction is 50% and the rest is filled with 1 M $LiPF_6$ electrolyte. The initial concentration of lithium ion is uniform in the NMC electrode with a state of charge at 2% which corresponds to about 4.1V vs. Li. We discharge the cell at a current density of 240 A/m^2 (per current collector area) until the terminal voltage reaches 3.5 V. We would like to distribute the NMC material, i.e., control the volume fraction in the domain, to maximize the specific energy during the discharge process.

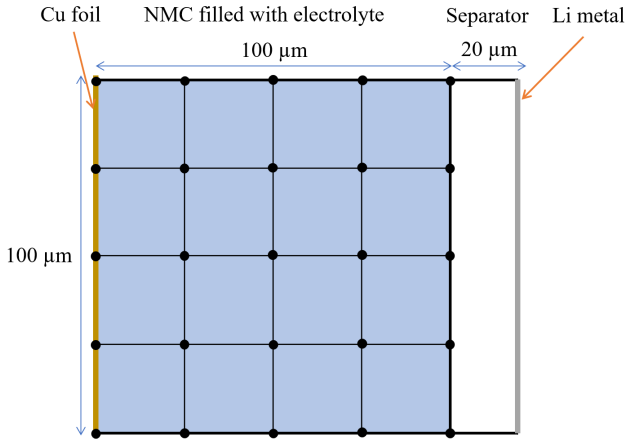

Figure 1. The domain and mesh for material distribution optimization.

Mathematically, this problem is formulated by

$$\max_{\rho} E(\rho)$$
$$\begin{cases} \int_{\Omega} \rho(\mathbf{x}) \mathrm{d}V = \rho_0 \int_{\Omega} \mathrm{d}V \\ \rho(\mathbf{x}) \in [0,1] \end{cases} \tag{1}$$

where $\rho = \rho(\mathbf{x})$ is the solid volume fraction at point $\mathbf{x}$, $\rho_0 = 0.5$ is the preset average solid volume fraction in the entire domain, $E(\rho)$ is the discharge energy of the cell. We discretize the domain by a 5×5 mesh to represent the material distribution by 25 nodal variables, i.e., $\boldsymbol{\rho} = (\rho_1, \rho_2, \ldots, \rho_N)$ where N=25. Then Eq. (1) becomes

$$\max_{\boldsymbol{\rho}=(\rho_1,\rho_2,\ldots,\rho_N)} E(\boldsymbol{\rho})$$
$$\begin{cases} \sum_{i=1}^{N} v_i \rho_i = \rho_0 \\ \rho_i \in [0,1], \quad i = 1,\ldots,N \end{cases} \tag{2}$$

where v_i denotes the weight of integration to confine the average volume fraction of solid material to be ρ_0.

The energy $E(\boldsymbol{\rho})$ is evaluated by a pseudo three-dimensional model[5], which extends the pseudo two-dimensional model[6] by adding consideration of field variation in the lateral direction of the electrode. The governing equations in the NMC domain include the following.

The lithium ion diffusion in an active material particle is given by

$$\frac{\partial c_s}{\partial t} = \frac{D_s}{r^2}\frac{\partial}{\partial r}\left(r^2\frac{\partial c_s}{\partial r}\right), \tag{3}$$

where c_s is the lithium concentration in the solid (NMC), t is time, r is the radial coordinate along the particle radius and D_s is the solid diffusivity. The solid phase potential, Φ_s, is given by

$$\nabla \cdot (\sigma_{s,eff}\nabla\Phi_s) = a_s i, \tag{4}$$

where $\sigma_{s,eff} = \sigma_s\rho^{1.5}$ is the effective solid conductivity (σ_s is the bulk solid conductivity), $a_s = 3\rho/r_p$ is the active surface area per unit volume (r_p is the particle radius) and i denotes the intercalation current density. The lithium ion concentration in the electrolyte, c_e, is given by

$$\varepsilon\frac{\partial c_e}{\partial t} + \nabla \cdot (-D_{e,eff}\nabla c_e) = \frac{(1-t_+)}{F}a_s i\,, \tag{5}$$

where $D_{e,eff} = D_e\varepsilon^{1.5}$ is the effective electrolyte conductivity (D_e is the bulk electrolyte diffusivity while $\varepsilon = 1-\rho$ is the electrolyte volume fraction), t_+ is the transference number and F is the Faraday constant. The electrolyte phase potential, Φ_e, is given by

$$\nabla \cdot \left\{-\kappa_{e,eff}\left[\nabla\Phi_e - \frac{2RT}{F}\left(1+\frac{\mathrm{d}\ln f_{\pm}}{\mathrm{d}\ln c_e}\right)(1-t_+)\nabla\ln c_e\right]\right\} = a_s i\,, \tag{6}$$

where $\kappa_{e,eff} = \kappa_e\varepsilon^{1.5}$ is the effective electrolyte conductivity (κ_e is the bulk electrolyte conductivity), R is the gas constant, T is temperature and $f_{\pm}$ is the electrolyte activity coefficient. The current density i is given by the Butler-Volmer equation

$$i = i_0\left[\exp\left(\frac{\alpha F\eta}{RT}\right) - \exp\left(\frac{(1-\alpha)F\eta}{RT}\right)\right], \tag{7}$$

where i_0 is the exchange current density, α is anodic charge transfer coefficient and η is the over-potential calculated by

$$\eta = \Phi_s - \Phi_e - U^0\,, \tag{8}$$

where U^0 is the equilibrium potential of the NMC material.

In the separator domain, Eqs. (5) and (6) still hold except i=0 since there is no intercalation.

The energy $E(\boldsymbol{\rho})$ is calculated by

$$E(\boldsymbol{\rho}) = \int_0^{t_0} i_{app} U(\boldsymbol{\rho}, t)\,\mathrm{d}t\,, \tag{9}$$

where $i_{app} = 240\ \mathrm{A/m^2}$ is the discharge current density, $U(\boldsymbol{\rho}, t)$ is the terminal voltage of the cell and t_0 is the end time of discharge. The cut-off voltage window is $U(\boldsymbol{\rho}, 0) = 4.1$ V and $U(\boldsymbol{\rho}, t_0) = 3.5$ V. The equations above are solved by the finite element method (FEM) using COMSOL Multiphysics 5.4. Material properties are taken with the default values in the material database. Note that the mesh for FEM calculation is much finer than the optimization mesh.

The discharge energy depends on the solid volume fraction, and we want to find the maximum. This type of material distribution problem belongs to the field of topology optimization, which has been under development since 1988.[7,8] Typical optimization approaches require gradient-based optimizers. However, for the transient and non-linear problem here, the gradient cannot be efficiently obtained. We use an innovative DNN-boosted stochastic method[4] to solve Eq. (2), as shown in Figure 2.

We set the number of incremental training samples to be $n = 100$. For the initial batch, 100 random arrays of $\boldsymbol{\rho}$ satisfying the constraints in Eq. (2) are generated. These data together with their corresponding energy values $E(\boldsymbol{\rho})$ calculated by FEM are used as the training data and inputted into the DNN. After training, the network at this stage has a certain level of abilities to predict the energy values. Next, the maximum energy is obtained by GSA with $E(\boldsymbol{\rho})$ estimated by the DNN instead of solving differential equations by FEM. After obtaining the optimized solution $\boldsymbol{\rho}_{base}$, more training data are generated by adding some noise to $\boldsymbol{\rho}_{base}$. The disturbance added to the solution includes replacing one or several entries with random numbers, exchanging several values in the matrix and switching rows and columns. After constraints are checked and enforced, a new batch of 100 training samples selected among the disturbed $\boldsymbol{\rho}_{base}$ are generated by FEM calculations. These new training samples are close to the optimized solution region, so that they are more efficient to train the DNN to predict better at the region of interest. The self-directed learning and optimization process stops when the value of the objective function does not change any more.

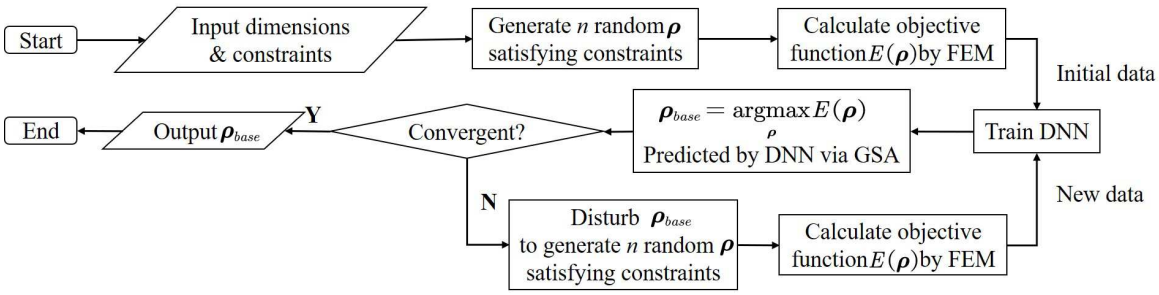

Figure 2 Flow diagram of the optimization algorithm

Results

Our baseline solution is the uniform electrode with $\boldsymbol{\rho}_0 = (0.5,0.5,\ldots,0.5)$. The energy is calculated to be $E(\boldsymbol{\rho}_0) = 160\ \mathrm{kW/m^2}$ (based on current collector area). We define a dimensionless energy $\tilde{E}(\boldsymbol{\rho}) = E(\boldsymbol{\rho})/E(\boldsymbol{\rho}_0)$. The convergence plot is shown in Figure 3. As the accumulated number of FEM calculations increases, more data are fed to the DNN to improve its prediction accuracy. The difference of the two curves reflects the DNN's prediction error. It can be seen that despite some small prediction error, DNN gives an excellent guidance on the search direction. In fact, it is not necessary for the DNN to be exactly precise in predicting the $E(\boldsymbol{\rho})$ value to guide finding the optimized $\boldsymbol{\rho}$. The algorithm converges at $n_{FEM} = 900$ with $\max \tilde{E}(\boldsymbol{\rho}) = 1.18$. The corresponding solution, i.e., optimal material distribution, is presented in Figure 4.

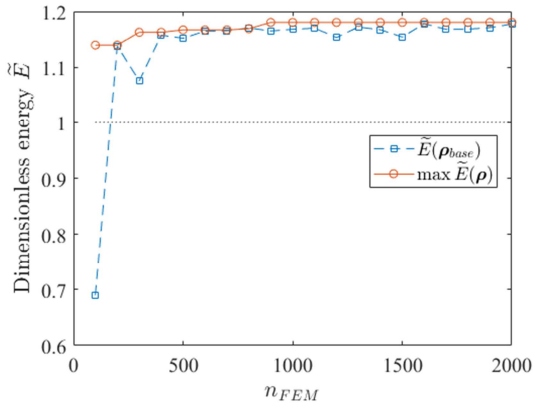

Figure 3 Optimal dimensionless energy vs. accumulated number of FEM calculations invoked to generate the training data during the optimization process. $\tilde{E}(\boldsymbol{\rho}_{base})$ denotes the energy of DNN-predicted solution, while $\max \tilde{E}(\boldsymbol{\rho})$ denotes the maximum energy value among the accumulated n_{FEM} FEM samples.

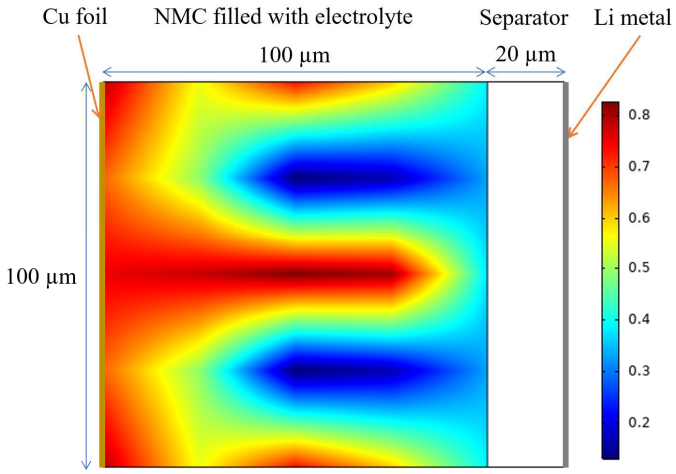

Figure 4 Optimal distribution of solid volume fraction ρ (pattern at n_{FEM}= 900). The pattern does not show any change after further calculations. The red color means dense, low porosity NMC while the blue color means electrolyte with little or no NMC.

We can see from Figure 4 that the optimized distribution shows a finger-like periodic pattern. The electrode is continuous near the current collector with fingers facing the separator. Physically, the channels between the fingers, which are filled with electrolytes,

facilitate lithium ion transport and intercalation/deintercalation. This helps reducing the associated polarization and therefore delivers a larger discharge capacity at a given discharge current density.

Conclusions

In this paper, we show a method to obtain the optimal geometry or topology of porous electrode without any assumptions on its pattern. We consider a two-dimensional NMC electrode with lithium metal as the counter electrode. This problem is formulated as topology optimization and solved by self-directed online machine learning. Our method produces an electrode pattern with the specific energy about 18% higher than that of a uniform electrode. This highlights the potential of freeform geometry optimization in battery design.

Acknowledgments

This work is supported by National Science Foundation under Grant No. CNS-1446117.

References

1. V. Etacheri, R. Marom, R. Elazari, G. Salitra, and D. Aurbach, *Energ Environ Sci*, **4**, 3243–3262 (2011).
2. F. Shen et al., *Adv Energy Mater*, **6**, 1600377 (2016).
3. G. T. Teixidor, B. Y. Park, P. P. Mukherjee, Q. Kang, and M. J. Madou, *Electrochim Acta*, **54**, 5928–5936 (2009).
4. C. Deng, C. Qin, and W. Lu, *arXiv preprint*, *arXiv:2002.01927* (2020).
5. B. Wu and W. Lu, *J Power Sources*, **360**, 360–372 (2017).
6. B. Wu, S. Han, K.G. Shin, and W. Lu, *J Power Sources*, **395**, 128-136 (2018).
7. M. P. Bendsøe and N. Kikuchi, *Comput Method Appl M*, **71**, 197–224 (1988).
8. G. I. N. Rozvany, *Struct Multidiscip O*, **37**, 217–237 (2009).